

Two tractable models of dynamic resonances and their application to Fano resonances at light scattering

Michael I. Tribelsky*

*M. V. Lomonosov Moscow State University,
Faculty of Physics, Moscow, 119991, Russia[†]*

Andrey E. Miroschnichenko[‡]

*University of New South Wales Canberra,
School of Information and Information Technology, ACT, 2600, Australia*

(Dated: September 20, 2022)

Abstract

We study numerically and analytically effects of resonant light scattering by subwavelength high-index particles with weak dissipation in the vicinity of the destructive interference at Fano resonances. We show that sharp variations in the envelope of the incident pulse may initiate unusual, counterintuitive dynamics of the scattering associated with interference of modes with fast and slow relaxation. In particular, we observe and explain intensive sharp spikes in scattering cross section just behind the leading and trailing edges of the incident pulse. The latter occurs when the incident pulse is over and is explained by the release of the electromagnetic energy accumulated in the particle at the previous stages of the scattering. To mimic the numerical results, we develop two tractable analytical models. Both reproduce with high accuracy all the dynamic effects of the numerics. The models allow us to reveal the physical grounds for the spikes explained by the violation of balance between the resonant and background partitions during the transient. Besides, we compare the models with each other and reveal their mutual advantages and disadvantages.

Keywords: Fano resonances, Mie scattering, resonant interference, transient response.

I. INTRODUCTION

High- Q resonances are of utmost importance in a wide diversity of problems. It is explained by the fact that the corresponding resonance should have a high Q -factor to obtain strong resonant effects. However, the characteristic relaxation time for a resonance is inversely proportional to its Q -factor. Thus, the price one must pay for making use of high- Q resonances is long-lasting transient effects. On the other hand, the frontier of modern photonics moves toward short and ultrashort pulses. Nowadays, these two factors together make typical the situation, when the duration of a laser pulse becomes comparable or even shorter than the relaxation times of the resonant effects initiated by this pulse. It means that the theoretical description of these resonant phenomena based on steady-state approximations becomes erroneous and should be revised thoroughly.

It is well-known that non-steady resonant scattering may qualitatively differ from its

* mitribel@gmail.com

† Also at National Research Nuclear University MEPhI (Moscow Engineering Physics Institute), Moscow, 115409, Russia

‡ andrey.miroshnichenko@unsw.edu.au

steady-state realizations and exhibits new effects, which do not exist in the steady-state case, see, e.g., Ref. [1]. However, the corresponding study in subwavelength optics has begun only recently [2-4].

This paper presents a general approach to the theoretical description of non-steady resonant light scattering by subwavelength particles based on the extension of the Mie solution to this case. We apply it to inspect the light scattering by a cylinder. We show that non-steady resonant scattering of light may exhibit counterintuitive new effects, and the scattering field patterns, in this case, may have very little in common with the one for the steady-state scattering. Besides the purely academic interest, the results obtained may be employed to design a new generation of fast, multifunctional nanodevices.

The *ab initio* description of the non-steady resonant light scattering is possible only by numerical integration of the complete set of Maxwell's equations. Nowadays, due to the existence of plenty of pieces of software, both free and commercial, created to perform this integration, the integration has become a more or less routine procedure. However, to find in the range of the problem parameters a windows, where a desired effect is the most pronounced, the dependence of the scattering on these parameters in a wide domain of their variations is required. To this end, numerical methods are not appropriate, and analytically tractable models are required. To the best of our knowledge, for the time being, none of them exists.

Here, we present two such models, apply them to describe non-steady Fano resonances, and compare the results with direct numerical integration of the complete set of Maxwell's equations discussed in Ref. [1]. The comparison indicates the high accuracy of both models and reveals their mutual advantages and disadvantages. The models unveil the physical grounds for the counterintuitive spikes in the scattered radiation observed behind the leading and trailing edges of the incident pulse.

The first model is based on the temporal coupled-mode theory (TCMT) [2] generalized to applications to essentially non-steady scattering. The second model mimics non-steady resonant vibrations by a superposition of dynamics of driven harmonic oscillators (HO). The latter approach looks similar to the harmonic inversion, see, e.g., Ref. [3-5]. However, in our case, the mode selection for the approximation and, most importantly, the choice of the values of the model parameters are based on the system in question's physical properties. Thus, it reveals the role of different excitations in the system dynamic and sheds light on

the physical nature of the system as a whole. Besides, this makes it possible to reduce the number of modes to be studied just to a few with non-trivial dynamics.

The paper has the following structure: In Sec. 2 the problem formulation is presented. Sec. 3 is devoted to the problem analysis and discussion of the obtained results. In Sec. 4 we formulate conclusions. Cumbersome details and expressions as well as several plots illustrating the developed approach are moved to Appendix.

II. PROBLEM FORMULATION

A. Preliminary

The simplest exactly solvable light scattering problems correspond to the steady-state scattering of a linearly polarized plane wave by a homogeneous sphere (the Mie solution) or infinite circular cylinder. In these solutions, the scattered field is presented as an infinite series of partial waves (dipole, quadrupole, etc.), also called multipoles [6]. Here, we generalize this approach to dynamic light scattering. It makes it possible to study quite intricate transient features.

One of the most typical resonant responses in light scattering by finite obstacles is the Fano resonance. A characterizing it asymmetric lineshape is explained by either constructive (the maximal scattering) or destructive (the minimal scattering) interference occurring close to each other in the frequency domain. The interfering parties are the so-called resonant (narrow line) and background (broad line) partitions of the same multipole. The narrow-line and broad-line partitions correspond to excitations with slow and fast relaxation time in the time-domain, respectively.

Naturally, the procedure of splitting a single partial wave into the two partitions is not unique. Accordingly, there are two main equivalent approaches to it. In the first approach, a partial wave is presented as a sum of the radiation of the conventional electric and toroidal multipoles [7]. However, in what follows, it will be more convenient for us to employ another approach. The resonant partition is associated with the corresponding electromagnetic mode excited in the bulk of the particle (volume polariton). In contrast, the background partition corresponds to the radiation of the surface current induced by the same incident wave scattered by the particle with the same geometrical shape but made of a hypothetical

material called the perfect electric conductor (PEC) [8].

At steady-state scattering, at a point of the destructive interference, the two partitions cancel each other. As a result, the contribution of the corresponding multipole is suppressed. For a subwavelength particle, when just a few first multipoles produce the overwhelming contribution to the overall scattering, the suppression even of one of them may reduce the scattering cross section dramatically [8]. However, since, as has been mentioned above, the resonant and background partitions are characterized by substantially different relaxation times, it is evident that during transient regimes, the mutual cancelation does not occur. Therefore, the violation of the destructive interference conditions must give rise to a considerable increase in the scattering intensity during the transient and other unusual effects. Some of them have already been discussed in our previous publications [9, 10].

We stress that though this increase in the scattering intensity looks similar to the well-known overshoot effect when a driven high- Q oscillator exhibits oscillatory relaxation to the steady-state, the physical grounds for the former is entirely different: If the overshoot is related to vibrations of a *single* oscillator, the discussed effect is explained by a superposition of *two different* oscillations. This distinction in the physical nature of the two cases gives rise to the corresponding difference in their manifestations. In particular, the amplitude of the scattering spike relative to that of the steady-state may be *in orders of magnitude* larger than that exhibited by the overshoot.

Thus, the dynamic resonant light scattering is a new and, practically, untouched subfield. Plenty of exciting effects hidden there are still undiscovered. In the present paper, we continue to explore this appealing topic.

To understand typical main features of the phenomenon, we consider the simplest problem formulation, namely the scattering of a rectangular incident pulse with duration τ , carrier frequency ω and temporal dependence of the fields $\sim \exp(-i\omega t)$ by an infinite circular cylinder with the base radius R and complex refractive index $m = n + i\kappa$. The amplitudes of the electromagnetic fields $A(t) = A_0 = \text{const} \neq 0$ inside the pulse and zero outside it. The refractive index of the surrounding cylinder medium equals unity. The cylinder is nonmagnetic, so its permeability $\mu = 1$. For further simplification, just the TE polarization and normal incidence are considered, see Fig. 1(a).

B. Instantaneous scattering cross section

In the conventional steady-state case, the scattering is quantitatively described by the cross section C_{sca} calculated per unit of length of the cylinder. C_{sca} is defined as the ratio of the integral power flux through a closed remote surface surrounding the scatterer to the intensity of the incident light. At non-steady scattering, both these quantities are time-dependent, and their ratio is not a constant anymore. Moreover, the ratio depends on the shape and position of the surface used to calculate the flux since the speed of light is finite.

To describe non-steady scattering, we introduce the *instantaneous* scattering cross section $C_{\text{sca}}(t)$ as the ratio of the instantaneous value of the power flux through a cylindrical surface, coaxial with the scattering cylinder and lying in the far wave zone, calculated per a unit of length of the cylinder, to the constant intensity of the rectangular incident pulse I_0 [1]. In a more general case, when the pulse envelope has a time-dependent shape $I(t)$, the scattered flux may be normalized over, e.g., the maximal value of $I(t)$, i.e., $I_0 = \text{Max}_t\{I(t)\}$.

The corresponding dimensionless scattering efficiency, $Q_{\text{sca}}(t)$ is connected with $C_{\text{sca}}(t)$ by the usual relation $Q_{\text{sca}}(t) = C_{\text{sca}}(t)/(2R)$, where R is the radius of the base of the cylinder. We also do not perform the time averaging of the Poynting vector over the period of oscillations.

The exact solution describing the steady-state scattering is built as an infinite series of partial waves (multipoles). For the problem in question, the complex amplitudes of the multipoles (scattering coefficients) associated with the outgoing partial waves a_ℓ and the field within the cylinder d_ℓ are given by the well-known expressions presented in Appendix Eq. (A.2), see also, e.g., [6]. Here ℓ designates the multipole order (dipole, quadrupole, etc.).

For the given problem, the scattering coefficients satisfy the identity [11]:

$$a_\ell \equiv a_\ell^{(\text{PEC})} - \frac{J'_\ell(mx)}{H_\ell^{(1)'}(x)} d_\ell; \quad a_\ell^{(\text{PEC})} \equiv \frac{J'_\ell(x)}{H_\ell^{(1)'}(x)}, \quad (1)$$

where $x = kR$ stands for the size parameter; $k = \omega/c$; c is the speed of light in a vacuum; $J_\ell(z)$ and $H_\ell^{(1)}(z)$ designate the Bessel and Hankel functions, respectively; prime denotes the derivative over the entire argument of a function; and $a_\ell^{(\text{PEC})}$ is the scattering coefficient of the same cylinder made of the perfect electric conductor.

Routine calculations result in the following expressions [1]:

$$Q_{\text{sca}} = Q_{\text{sca}}^{(0)} + Q_{\text{sca}}^{(\text{osc})} = \sum_{\ell=-\infty}^{\infty} \left\{ Q_{\text{sca}(\ell)}^{(0)} + Q_{\text{sca}(\ell)}^{(\text{osc})} \right\}, \quad (2)$$

$$Q_{\text{sca}(\ell)}^{(0)} = \frac{2}{x} |a_{\ell}|^2; \quad Q_{\text{sca}(\ell)}^{(\text{osc})} = -\frac{i}{x} [a_{\ell}^2 e^{2i(kr-\omega t)} - c.c.], \quad (3)$$

Here $Q_{\text{sca}}^{(0)}$ is the conventional scattering efficiency, while $Q_{\text{sca}}^{(\text{osc})}$ is an additional rapidly oscillating in time and space term with zero average.

C. Fano resonances

The Fano resonances [12–14] are a good example demonstrating unusual, counterintuitive effects in transient processes of resonant light scattering. For the steady-state scattering, their detailed discussion is presented, e.g., in Ref. [11]. Though in that paper, a spherical particle is considered, generalization to the case of a cylinder is a straightforward matter.

As it has been mentioned above, a key point of the Fano resonances is a presentation of the scattered wave as a sum of two partitions: resonant and background. In the proximity of the resonance the amplitude and phase of the former have a sharp ω -dependence, while for the latter its ω -dependence is weak. An important conclusion following from the results of Ref. [11] is that the splitting of a_{ℓ} into the two terms, given by Eq. (1), actually, is the singling out the background ($a_{\ell}^{(\text{PEC})}$) and resonant ($-\frac{J'_{\ell}(mx)}{H_{\ell}^{(1)'}(x)} d_{\ell}$) partitions.

Our goal is to recover the full time-dependence $Q_{\text{sca}}(t)$. For high- Q resonances, which we are interested in, the characteristic time scales of the transients should be large relative to the period of the field oscillations $2\pi/\omega$. Then, a quasi-steady approximation may be employed. It implies the same structure of the solution as that for steady-state scattering. However, now the scattering coefficients are regarded as *slowly-varying* functions of time. Let us apply this assumption to the TCMT and HO.

D. TCMT

In the specified case, the TCMT equations read as follows, see, e.g., Ref. [15]:

$$\frac{dp(t)}{dt} = -(i\omega_0 - \gamma) p(t) + \kappa s^+(t) \quad (4)$$

$$s^-(t) = B s^+(t) + \zeta p(t) \quad (5)$$

Here $s^+(t)$ and $s^-(t)$ are the amplitudes of the incoming (converging) and outgoing (diverging) cylindrical waves, respectively; B is the background reflection coefficient; κ and ζ are coupling constants; $p(t)$ describes the internal resonant mode excitation; and $\hat{\omega}_0 \equiv \omega_0 + i\gamma$ is the nearest pole of the scattering coefficients in the plane of complex $\hat{\omega}$. It is important to stress that for the selected temporal dependence $\sim \exp(-i\omega t)$ decaying modes must have $\gamma < 0$. Then, *the corresponding poles are situated in the lower semiplane.*

The analysis of Eqs. (4), (5) performed in Ref. [15] for the steady-state scattering indicates that $\kappa = \zeta = \sqrt{2|\gamma|} \exp(i\theta)$; $B = \exp(i\phi)$ and $\theta = (\phi + \pi)/2 + n\pi$, where n is an arbitrary integer. In this case the steady-state scattering coefficient $a_\ell^{(\text{TCMT})}$ is defined as $[s^-(t) - s^+(t)]/(2s^+(t))$. Eventually, it gives rise to a certain expression for $a_\ell^{(\text{TCMT})}$, where phase ϕ remains undefined yet. The authors of Ref. [15] fix it by fitting the profile $|a_\ell^{(\text{TCMT})}(\omega)|^2$ to $|a_\ell(\omega)|^2$ obtained from the steady-state exact solution. However, any fitting procedure is ambiguous since its results depend on the fitting window's size.

Meanwhile, there are other ways to fix ϕ , free from this disadvantage. In this paper we fix ϕ from the condition $|a_\ell^{(\text{TCMT})}(\omega)| = |a_\ell(\omega)|$ at the carrier frequency of the incident pulse. This gives rise to a quadratic equation, whose solution results in two values of ϕ in the non-trivial domain $-\pi \leq \phi \leq \pi$. The final choice is made based on the better overall coincidence of the two profiles. Such a choice is a straightforward matter, see Appendix.

The next difficulty is that the employed expression for $a_\ell^{(\text{TCMT})}$ is valid for the steady-state scattering solely. The latter is evident if we consider, e.g., the case when the incident pulse is already over, i.e., $s^+(t) = 0$. At the same time, the particle still radiates the accumulated electromagnetic energy, so that $s^-(t) \neq 0$. In this case, the discussed expression diverges. To avoid this difficulty, we have to redefine $a_\ell^{(\text{TCMT})}$. For the considered rectangular pulse, it may be done as follows: $a_\ell^{(\text{TCMT})}(t) = \frac{1}{2A_{0(\ell)} \exp(-i\omega t)} [s^-(t) - s^+(t)]$, where $A_{0(\ell)}$ is a constant amplitude of a converging incident cylindrical wave, corresponding to a given multipolarity. This definition coincides with the above one for the steady-state scattering but remains finite at $s^+(t) = 0$. In an arbitrary pulse shape, the role of $A_{0(\ell)}$ may play the corresponding maximal value.

Regarding $Q_{\text{sca}}(t)$, since in the discussed quasi-steady approximation the solution retains the same structure as that for the steady-state; i.e., Eqs. (2), (3) still remain valid but the replacement $a_\ell \rightarrow a_\ell^{(\text{TCMT})}(t)$ is required. As for the dependence $a_\ell^{(\text{TCMT})}(t)$, it is readily obtained by integration of Eq. (4) with the initial condition $p(0) = 0$:

$$a_\ell^{(\text{TCMT})}(t) = \frac{i\gamma [1 - e^{i\phi} (2e^{it(\omega-\omega_0)+\gamma t} - 1)] + (e^{i\phi} - 1)(\omega - \omega_0)}{2(\omega - \omega_0 - i\gamma)} \quad (6)$$

at $0 \leq t \leq \tau$ and

$$a_\ell^{(\text{TCMT})}(t) = \frac{i\gamma (e^{-\gamma\tau - i(\omega-\omega_0)\tau} - 1) e^{i[(\omega-\omega_0)t+\phi]+\gamma t}}{\omega - \omega_0 - i\gamma}, \quad (7)$$

at $t > \tau$ (remember that $\gamma < 0$). Note, that $a_\ell^{(\text{TCMT})}(t)$ given by Eqs. (6), (7) are indeed slowly-varying relative to $\exp(-i\omega t)$ since in the vicinity of a high- Q resonance $|\omega - \omega_0| \ll \omega$ and $|\gamma| \ll \omega$.

Another point to be stressed is that $a_\ell^{(\text{TCMT})}(t)$ given by Eqs. (6), (7) is not continuous at $t = 0$ and $t = \tau$: At $t = 0$ it has a jump from zero at $t = -0$ to $(\exp[i\phi] - 1)/2$ at $t = +0$. At $t = \tau$ the jump has the same value but the opposite sign. These discontinuities are a direct consequence of Eq. (5), which implies that the background scattering follows the variations of $s^+(t)$ instantaneously, without any delay.

E. Harmonic oscillators

Another model is based on the well-known fact that any linear oscillatory dynamic may be approximated by that of a system of driven coupled harmonic oscillators. We just have to apply it to the problem in question. The general solution of the equations for driven coupled HO has the form (see, e.g. [16])

$$z_k(t) = z_{ks}(t) + \sum_n C_n \Delta_{nk} e^{-i\hat{\omega}_n t}, \quad (8)$$

where $z_k(t)$ is a complex coordinate of the k -th oscillator; $\Delta_{nk} e^{-i\hat{\omega}_n t}$ and $\hat{\omega}_n$ stand for the corresponding eigenvector and complex eigenfrequency, respectively; $z_{ks}(t)$ is a particular solution, for a given drive, and C_n are the constants of integration defined by the initial conditions. An important point is that if the eigenvectors are selected as new variables (normal modes), the corresponding system of equations is diagonalized, i.e., each term in the sum in Eq. (8) evolves *independently* of the others and its dynamic is described by that of a *single* oscillator [16].

The main idea of the adaptation of Eq. (8) for a drive with a carrier frequency ω is that only the dynamics of the resonant eigenmodes with the frequency mismatch $|\omega - \text{Re} \hat{\omega}_n|$ of

the order of $|\text{Im} \hat{\omega}_n|$ or smaller than that are modeled. All other off-resonant eigenmodes are supposed to follow the drive adiabatically, obeying the quasi-steady approximation. This approach is reasonable, provided the contribution of the resonant modes to the overall dynamic is overwhelming. Fortunately, this is the case in most resonant phenomena in subwavelength optics and related problems.

Next, according to what just has been said, for the problem in question the eigenmode dynamic is described by the equation:

$$\ddot{f} - 2\gamma\dot{f} + \omega_0^2 f = A_0[\theta(t) - \theta(t - \tau)] \exp[-i\omega t]; \quad (\gamma < 0), \quad (9)$$

supplemented with the initial conditions $f(0) = \dot{f}(0) = 0$, where dot stands for d/dt and $\theta(z)$ is the Heaviside step function.

Eq. (9) has the following exact solution:

$$f(t) = A_0 e^{-i\omega t} \frac{e^{(i\omega + \gamma)t} [\omega_{0\gamma} \cos(\omega_{0\gamma} t) - (\gamma + i\omega) \sin(\omega_{0\gamma} t) +] - \omega_{0\gamma}}{(\omega^2 - \omega_0^2 - 2i\omega\gamma) \omega_{0\gamma}}, \quad (10)$$

at $0 \leq t \leq \tau$ and

$$f(t) = \frac{e^{\gamma(t-\tau)}}{\omega_{0\gamma}} \left\{ \left[\dot{f}(\tau) - \gamma f(\tau) \right] \sin \omega_{0\gamma}(t - \tau) + \omega_{0\gamma} f(\tau) \cos \omega_{0\gamma}(t - \tau) \right\}, \quad (11)$$

at $t > \tau$. Here $\omega_{0\gamma} \equiv \sqrt{\omega_0^2 - \gamma^2}$.

In what follows, we employ Eqs. (10), (11) to model the dynamics of the scattering coefficients. Naturally, for different coefficients the values of A_0 , ω_0 and γ are also different and will be defined below. The key equation now is Eq. (1), where the steady-state $a_\ell^{(\text{PEC})}$ and d_ℓ are replaced by $a_\ell^{(\text{PEC})}(t)$ and $d_\ell(t)$ and regarded as independent eigenmodes.

Let us stress the dramatic difference in the steady-state profiles $|d_\ell(x)|$ and $|a_\ell^{(\text{PEC})}(x)|$. If for the former the characteristic scale is of the order of $1/(mx) \ll 1$, for the latter it is just $1/x = O(1)$, see Eq. (1) and Ref. [11]. As a result, though in the vicinity of the maxima, the profiles $|d_\ell(x)|$ may be well-approximated by Lorentzians, this is not the case for $|a_\ell^{(\text{PEC})}(x)|$. Therefore, the actual dynamic of each PEC-mode may be quite far from that of a harmonic oscillator. Fortunately, since the characteristic scale in the time-domain is inverse of that in the ω -domain, the specified hierarchy of the scales means that the transients of the PEC-modes to the quasi-steady-state scattering is fast. In contrast, the ones for the resonant partitions are relatively slow. Accordingly, the approximation of the latter requires maximal accuracy. Regarding the possible errors in the approximation of the

dynamics of the PEC-modes, they are not crucial to the approach since due to the fastness of the PEC-modes, they affect just the very initial stage of the transient (a few periods $2\pi/\omega$, see below). To employ Eq. (9) for modeling the dynamics of the eigenmodes, we have to fix the values of the following four parameters: $\text{Re}[A_0]$, $\text{Im}[A_0]$, ω_0 and γ .

The approximation details are as follows: For the resonant d -modes the values of ω_0 and γ are given by the corresponding poles of $d_\ell(\omega)$ in the same manner as that in TCMT. Then, we require that at the drive frequency ω , the complex amplitude of the oscillator coincides with that for $d_\ell(\omega)$ of the exact solution.

The profile of a PEC-mode is far from a narrow resonant line. Therefore, the poles in the complex plane might have nothing to do with the dynamic of the mode. Then, ω_0 and γ become free parameters, and we need two more conditions to complete the problem. For them, we select (i) the equality of the frequencies maximizing the profile $|a^{(\text{PEC})}(\omega)|$ and the corresponding profile of the oscillator and (ii) the equality of the maxima themselves. This procedure fixes all four parameters of the HO-model unambiguously. For more details see Appendix.

III. RESULTS AND DISCUSSIONS

To illustrate the accuracy of the two models, their mutual advantages and disadvantages, we perform a comparison of their applications to the problem numerically studied in Ref. [1]. It is convenient to transfer to the dimensionless time: $t_{\text{new}} = t_{\text{old}}c/R$. Then, $\omega_{\text{new}} = \omega_{\text{old}}R/c \equiv x$. Since below only the dimensionless quantities are in use the subscript "new" will be dropped.

In Ref. [1] the following values of the parameters are employed: $\tau = 191.1$, $m = m_{\text{sim}} = 3.125$ and $x = x_{\text{sim}} = \omega_{\text{sim}} = 1.702$. The choice is done since this pair of m and x corresponds to a local minimum of $Q_{\text{sca}}^{(0)}$ associated with the destructive Fano resonances at $\ell = 0, \pm 2$, both of which are situated at the close vicinity of $x = x_{\text{sim}}$ ($x \approx 1.695$ for $\ell = 0$ and $x \approx 1.759$ for $\ell = \pm 2$).

For all other multipoles, x_{sim} corresponds to the off-resonant regions. Thus, only the dynamics of the modes with $\ell = 0, \pm 2$ should be approximated. Moreover, since the scattering coefficients differing only by the sign of ℓ are identical, the modes with $\ell = \pm 2$ may be regarded as a single one.

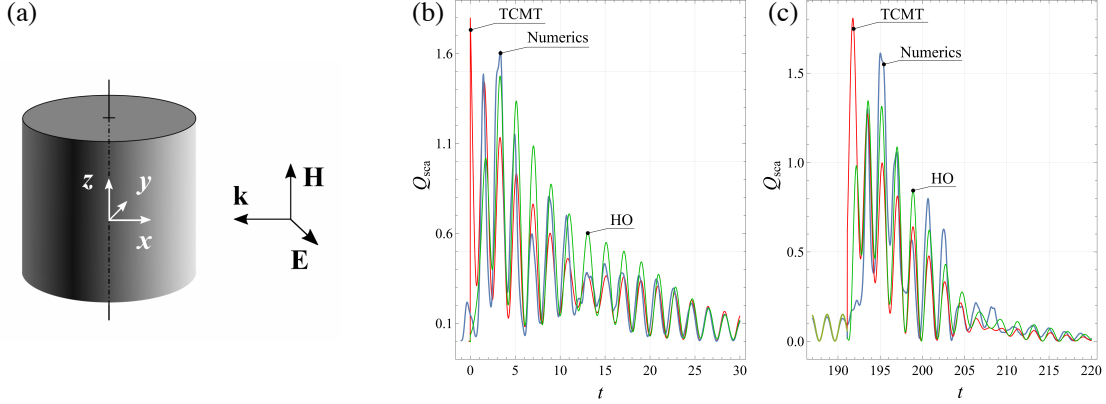


FIG. 1. (a) The mutual orientation of the cylinder, coordinate frame, and vectors \mathbf{k} , \mathbf{E} and \mathbf{H} of the incident linearly polarized plane wave. Spikes in scattering behind the leading (b) and trailing (c) edges of the rectangular incident pulse. Note the large amplitude of the spikes relative to that of the steady-state scattering. The latter is shown by the part of the plots (c) at $t < \tau$. A certain scattering at $t < 0$ exhibiting by the numerics in (a) is related to a smoothing of the rectangular envelope required for the code stabilization.

The poles of the scattering coefficients adjacent to ω_{sim} are

$$\hat{\omega}_0^{\ell=0} \approx 1.741 - 0.097i; \quad \hat{\omega}_0^{\ell=2} \approx 1.535 - 0.0614i; \quad (12)$$

For TCMT

$$\phi^{\ell=0}(\omega_{\text{sim}}) \approx -2.263, \quad \phi^{\ell=2}(\omega_{\text{sim}}) \approx 0.471, \quad (13)$$

For HO

d -modes: $\hat{\omega}_\ell$ are given by Eq. (12). Regarding A_0 ,

$$A_{0(d)}^{\ell=0} \approx -0.263 + 0.554i; \quad A_{0(d)}^{\ell=2} \approx 0.555 + 0.142i. \quad (14)$$

PEC-modes:

$$\hat{\omega}_{0(\text{PEC})}^{\ell=0} \approx 2.495 - 0.837i; \quad \hat{\omega}_{0(\text{PEC})}^{\ell=2} \approx 2.137 - 0.532i; \quad (15)$$

$$A_{0(\text{PEC})}^{\ell=0} \approx 3.811 - 0.979i; \quad A_{0(\text{PEC})}^{\ell=2} \approx -0.392 - 0.793i. \quad (16)$$

Note that, despite the error in the approximation of $a^{(\text{PEC})}$, the approximation of $a_\ell(\omega)$ in the vicinity of the Fano resonances is quite accurate, see Appendix.

The quantitative comparison of the two models with the numerics of Ref. [1] is shown in Fig. 1(b,c). The origin of the t -axis is shifted so that $t = 0$ corresponds to the moment when

the scattered radiation for the first time is detected by the measuring monitors situated in the far wave zone. The comparison exhibits the high accuracy of both models.

To get a quantitative criterion of the accuracy of the models in a given window $t_1 \leq t \leq t_2$ we do the following: The time in the window is sampled with a step δt . Then, the root mean square error (RMSE) for the difference $Q_{\text{sac}}^{\text{num}}(t) - Q_{\text{sac}}^{\text{mod}}(t)$ is calculated for the given sampling. Here $Q_{\text{sac}}^{\text{mod}}(t)$ designates the corresponding dependences for each model. At $\delta t \rightarrow 0$ the RMSE converges to a certain constant $\delta Q_{\text{sac}}(t_1, t_2)$, regarded as a measure of the model accuracy in the given window. For the two windows with essentially non-steady dynamics adjacent to the leading and trailing edges of the incident pulse ($t_1 = 0, t_2 = 37.5$ and $t_1 = \tau, t_2 = \tau + 37.5$, see Fig. 1(b,c)) $\delta Q_{\text{sac}}^{(\text{TCMT})} = 0.196$, $\delta Q_{\text{sac}}^{(\text{HO})} = 0.169$, and $\delta Q_{\text{sac}}^{(\text{TCMT})} = 0.157$, $\delta Q_{\text{sac}}^{(\text{HO})} = 0.129$, respectively ¹. Here superscripts HO and TCMT designate the corresponding models.

IV. CONCLUSIONS

Thus, though both models demonstrate high accuracy, the one of the HO-model is a little better than that of TCMT. In addition, while the TCMT-model just *describes* the complicated dynamics of the resonant light scattering, the HO-model also elucidates the physical grounds for the sharp intensive spikes in the scattering observed in the numerics behind the leading and trailing edges of the incident pulse: The spikes during the transient are explained by the violation of the balance between the resonant and background excitations. The violation, in turn, is caused by the difference in the corresponding relaxation times. Then, the uncompensated part of the interfering modes is exhibited as a spike. Note that if the "basement" of the scattered pulse is cut off at the level above the intensity of the steady-state scattering, the duration of the remaining parts of the spikes occurs very small. This procedure may be used as a new method of (ultra)short pulse generation at nanoscale.

Regarding possible extensions of the models, while the governing equations of TCMT are simpler than those of HO, the accuracy of the HO-model is higher relative to the one of TCMT. Besides, the implementation of the HO model is more straightforward and does not require a sophisticated procedure to connect the model's parameters with those of the

¹ The selected width of the window $\Delta t = 37.5$ satisfies the condition $\exp(-|\gamma|\Delta t) \approx 0.1$, where $|\gamma|$ is the smallest decrement corresponding to $\ell = 2$, see Eq. (12).

initial underlying problem.

If just a single resonant excitation is a concern, the HO-model may be used based even on fitting an experimentally obtained spectrum of the modules of the output signal. On the other hand, when the interference of several excitations is essential, its application implies knowledge of the phases, obtained either from an analytical solution or measured experimentally. While the latter is challenging in the optical range, it is a routine procedure at radio frequencies; see, e.g., [17, 18] and references therein. Thus, both models complement each other and may be very useful in descriptions of a wide variety of resonant phenomena.

ACKNOWLEDGMENTS

The authors are very grateful to Boris Y. Rubinstein for his valuable help in symbolic computer calculations.

M.I.T. acknowledges the financial support of the Russian Foundation for Basic Research (Projects No. 20-02-00086) for the analytical study, the Moscow Engineering Physics Institute Academic Excellence Project (agreement with the Ministry of Education and Science of the Russian Federation of 27 August 2013, Project No. 02.a03.21.0005) for the modeling of the resonant light scattering, as well as the contribution of the Russian Science Foundation for the computer simulation (Project No. 21-12-00151) and the provision of user facilities (Project No. 19-72-30012).

Appendix A: Scattering coefficients

The scattering coefficient for the problem under consideration read as follows:

$$a_\ell = \frac{mJ_\ell(mx)J'_\ell(x) - J_\ell(x)J'_\ell(mx)}{mJ_\ell(mx)H_\ell^{(1)'}(x) - H_\ell^{(1)}(x)J'_\ell(mx)}, \quad (\text{A.1})$$

$$d_\ell = \frac{2i/(\pi x)}{mJ_\ell(mx)H_\ell^{(1)'}(x) - H_\ell^{(1)}(x)J'_\ell(mx)}, \quad (\text{A.2})$$

Note that $a_\ell = a_{-\ell}$, $d_\ell = d_{-\ell}$, see Eqs. (A.1)–(A.2).

Appendix B: phase in the TCMT-model

To obtain the value of ϕ , note that according to Ref. [15] $a_\ell^{(\text{TCMT})}$ may be presented as

$$a_\ell^{(\text{TCMT})} = \frac{1}{2} \frac{i(\omega_0 - \omega)(e^{i\phi} - 1) + \gamma(1 + e^{i\phi})}{i(\omega_0 - \omega) - \gamma}. \quad (\text{B.1})$$

(the same expression may be obtained from Eq. (6), if we formally consider its limit at $t \rightarrow \infty$). Then, after some algebra Eq. (B.1) gives rise to the following expression for $|a_\ell^{(\text{TCMT})}|^2$:

$$|a_\ell^{(\text{TCMT})}|^2 = \sin^2 \frac{\phi}{2} \left| \frac{\cot \frac{\phi}{2} + \frac{\omega - \omega_0}{\gamma}}{1 + i \frac{\omega - \omega_0}{\gamma}} \right|^2 = \frac{1}{1 + q^2} \frac{(q + \epsilon)^2}{1 + \epsilon^2}, \quad (\text{B.2})$$

where $\epsilon = -(\omega - \omega_0)/\gamma$ and $q = -\cot(\phi/2)$. We remind that $\gamma < 0$. The last formula in Eq. (B.2) is the conventional Fano profile with the asymmetry parameter q [12–14].

Following the procedure described in the main text, we have to equalize $|a_\ell^{(\text{TCMT})}(\omega_{\text{sim}})|^2$ to $|a_\ell(\omega_{\text{sim}})|^2$, where $a_\ell(\omega_{\text{sim}})$ is given by Eq. (A.1) at $x = \omega_{\text{sim}}$ (remember that in the selected dimensionless variables x and ω numerically are equal to each other). This brings about a quadratic equation for q , whose solutions are

$$q_{(\pm)} = \frac{\epsilon_{\text{sim}} \pm (1 + \epsilon_{\text{sim}}^2) |a_\ell(\omega_{\text{sim}})| \sqrt{1 - |a_\ell(\omega_{\text{sim}})|^2}}{(1 + \epsilon_{\text{sim}}^2) |a_\ell(\omega_{\text{sim}})|^2 - 1}, \quad (\text{B.3})$$

where $\epsilon_{\text{sim}} = -(\omega_{\text{sim}} - \omega_0)/\gamma$. Note that for the problem in question $|a_\ell|$ always is smaller than unity, see, e.g., [19]. Therefore, the roots in Eq. (B.3) are always real.

Plots of $|a_\ell(\omega)|$ as well as their approximations at $q = q_{(+)}$, $q = q_{(-)}$ and $\ell = 0, 2$ at the values of ω_0 , γ given by Eq. ((12)) are shown in Fig. B.1. Thus, for $\ell = 0$ the better overall approximation is at $q = q_{(-)}$. For the case in question its numerical value is 0.4700, which corresponds to $\phi \approx -2.263$. In contrast, for $\ell = 2$ the better overall approximation is at $q = q_{(+)} \approx -4.172$, corresponding to $\phi \approx 0.471$.

Appendix C: The approximation procedure for the HO-model

A steady-state solution of Eq. (9) with the r.h.s equals $A_0 \exp[-i\omega t]$ is

$$f_s(t) = F_s(\omega) e^{-i\omega t}; \quad F_s(\omega) \equiv -\frac{|A_0| e^{i\varphi}}{\omega^2 - \omega_0^2 - 2i\gamma\omega}. \quad (\text{C.1})$$

Thus, to apply the HO-model to the discussed light scattering problem, the following model parameters should be fixed: the complex drive amplitude $A_0 \equiv |A_0| e^{i\varphi}$, the frequency ω_0

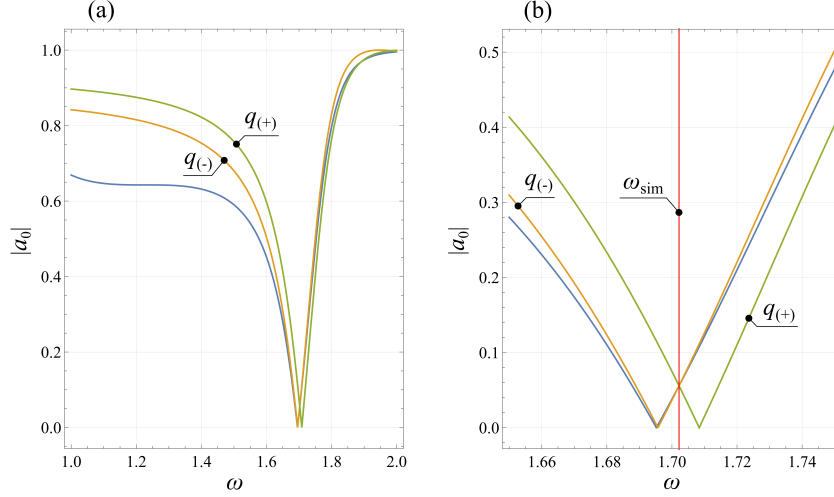


FIG. B.1. The approximation of the profile $|a_0(\omega)|$ shown as a blue line (unmarked) by Eq. (B.2) at $q = q_{(-)}$ and $q = q_{(+)}$. The general view (a) and the vicinity of $\omega = \omega_{\text{sim}}$ (b). Though all plots have the same value at $\omega = \omega_{\text{sim}}$, the overall approximation is better at $q = q_{(-)}$.

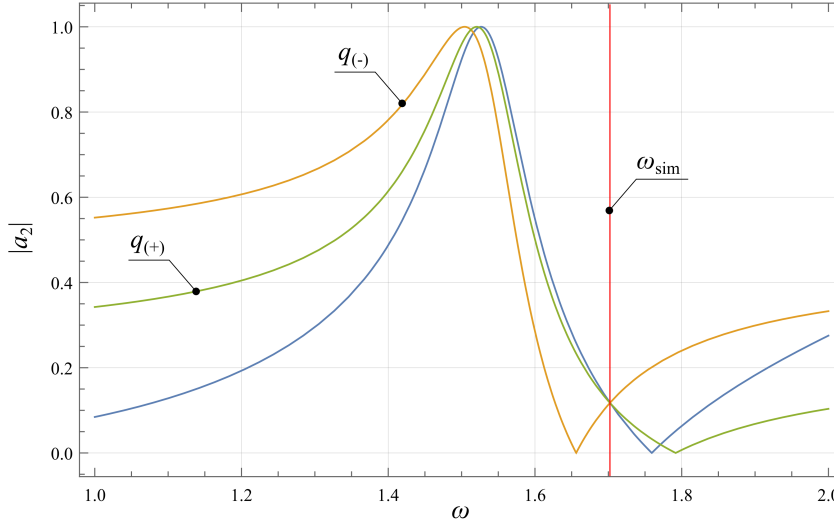


FIG. B.2. The same as that in Fig. B.1(a) for $\ell = 2$. The better overall approximation is for $q = q_{(+)}$

and the damping factor γ . In the case of the d -modes the values of ω_0 and γ are given by the position of the nearest to ω_{sim} complex pole of the steady-state coefficient $d_\ell(\omega)$. The remaining undefined parameters are A_0 is readily obtained from the equality $F_s(\omega_{\text{sim}}) = d_\ell(\omega_{\text{sim}})$.

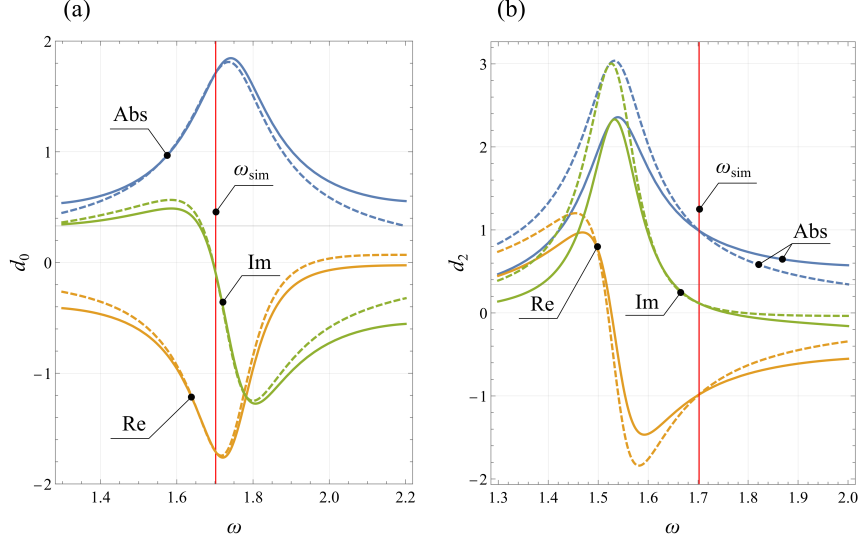


FIG. B.3. d -modes. Exact steady-state scattering coefficients (solid lines) and their approximations in the HO-model (dashed lines). Abs, Re and Im designate the modula, real and imaginary parts of the coefficients, respectively. The larger the difference between ω_{sim} and the resonant frequency maximizing $|d_\ell|$, the larger the approximation error, cf. panels (a) and (b).

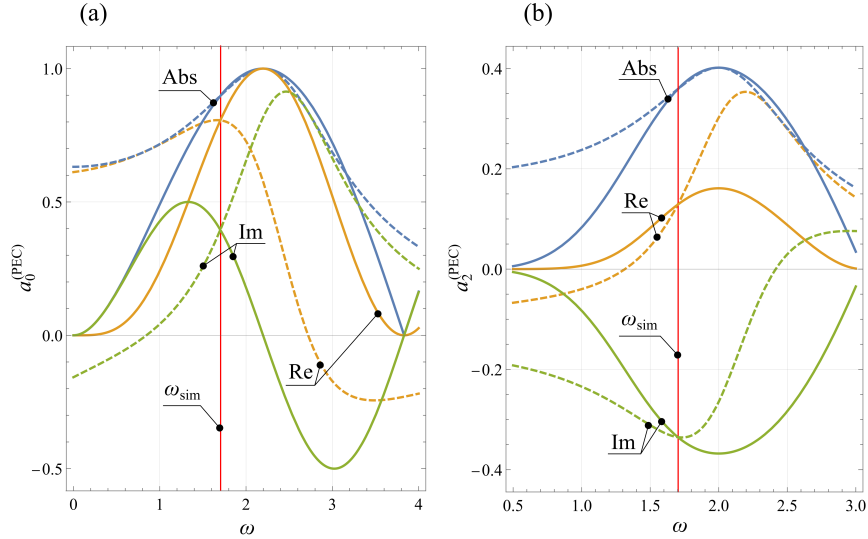


FIG. B.4. The same as that in Fig. B.3 for PEC-modes.

The case of the PEC-modes is more tricky since neither ω_0 , nor γ can be obtained in the same easy manner as that for the d -modes. Once again, it is convenient to present the

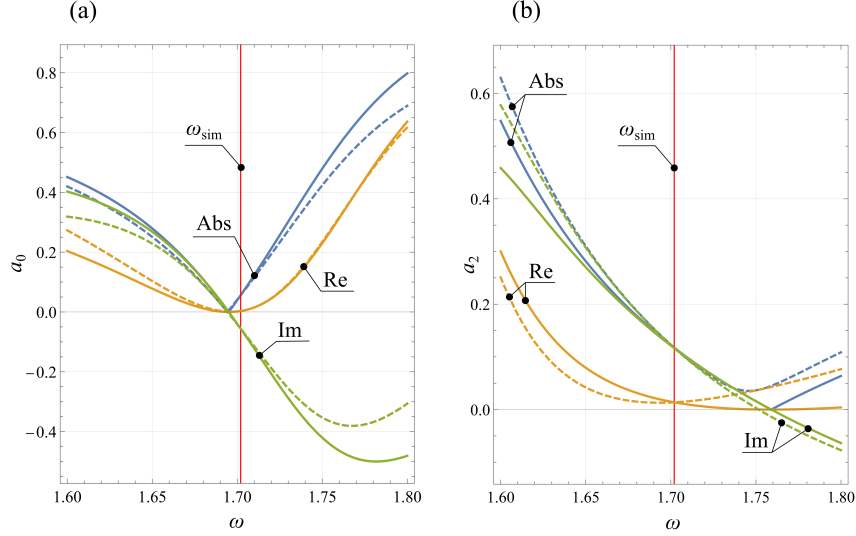


FIG. B.5. The same as that in Fig. B.3 for a -modes.

complex amplitude A_0 in the form $A_0 = |A_0|e^{i\varphi}$. Then, the maximum of $|F_s(\omega)|^2$ equals

$$\text{Max}_{\omega}\{|F_s(\omega)|^2\} \equiv |F_s|_{\text{max}}^2 = \frac{|A_0|^2}{4\gamma^2\omega_{0\gamma}^2}, \quad (\text{C.2})$$

and is achieved at

$$\omega = \omega_{\text{max}} \equiv \sqrt{\omega_0^2 - 2\gamma^2}. \quad (\text{C.3})$$

We remind that $\omega_{0\gamma} = \sqrt{\omega_0^2 - \gamma^2} = \sqrt{\omega_{\text{max}}^2 + \gamma^2}$, see Eqs. (9)–(11), (C.3). Let us consider ω_{max} as a new independent parameter instead of ω_0 . Next, according to the procedure described in the main text, we require that $\omega_{\text{max}} = \omega_{\text{max}(\ell)}^{(\text{PEC})}$, where $|a_{\ell}^{(\text{PEC})}(\omega_{\text{max}(\ell)}^{(\text{PEC})})|_{\text{max}}^2 \equiv |a_{\ell}^{(\text{PEC})}|_{\text{max}}^2$ is the maximal value of the corresponding quantity. This fixes the value of ω_{max} by the shape of the profile $|a_{\ell}^{(\text{PEC})}(\omega)|^2$.

The condition $|F_s|_{\text{max}}^2 = |a_{\ell}^{(\text{PEC})}|_{\text{max}}^2$ expresses $|A_0|^2$ in terms of γ . To fix γ we require that $|F_s(\omega_{\text{sim}})|^2 = |a_{\ell}^{(\text{PEC})}(\omega_{\text{sim}})|^2$, where ω_{sim} is the carrier frequency of the incident pulse. It gives rise to a biquadratic equation for γ . After some algebra, its only solution satisfying the condition $\text{Re } \gamma < 0$, $\text{Im } \gamma = 0$ may be presented in the following form:

$$\gamma = -\frac{\omega_{\text{max}}}{\sqrt{2}} \left\{ -1 + \sqrt{1 + \frac{(\omega_{\text{max}}^2 - \omega_{\text{sim}}^2)^2 |a_{\ell}^{(\text{PEC})}|_{\text{sim}}^2}{\omega_{\text{max}}^4 (|a_{\ell}^{(\text{PEC})}|_{\text{max}}^2 - |a_{\ell}^{(\text{PEC})}|_{\text{sim}}^2)}} \right\}^{1/2} \quad (\text{C.4})$$

where $|a_{\ell}^{(\text{PEC})}|_{\text{sim}}^2 \equiv |a_{\ell}^{(\text{PEC})}(\omega_{\text{sim}})|^2$. Nonnegativity of the expressions under the signs of radicals is seen straightforwardly.

Now, the last unfixed parameter φ is readily obtained from the condition that the phase of $a_\ell^{(\text{PEC})}(\omega_{\text{sim}})$ equals the one of $F_s(\omega_{\text{sim}})$. The values of $|a_\ell^{(\text{PEC})}|_{\text{max, sim}}^2$ and $\omega = \omega_{\text{max}}^{(\text{PEC})}$ are obtained numerically according to the definition of $a_\ell^{(\text{PEC})}$, see Eq. (1).

The application of this procedure results in the values of the parameters presented in the main text, see Eqs. (15) and (16). Note that while the approximation errors for the PEC modes is large, the final approximations for a_ℓ in the proximity of ω_{sim} are quite accurate, cf. Figs. B.4 and B.5.

Next, there are some points, where $|a_\ell^{(\text{PEC})}(\omega)|$ vanishes, see, e.g., Fig B.4(a). If ω_{sim} coincides with such a point, i.e., $|a_\ell^{(\text{PEC})}(\omega)| = 0$, the phase of $a_\ell^{(\text{PEC})}(\omega)$ is indeterminate, and our method to fix the complete set of the HO-model parameters seemingly fails. However, in this case, A_0 in the r.h.s. of Eq. (9) should be set to zero, the PEC-mode does not contribute to the model dynamic, and the corresponding parameters merely are not required.

Another point of a special interest is the one, when $\omega_{\text{sim}} = \omega_{\text{max}}$. In this case the straightforward application of Eq. (C.4) gives rise to an indeterminate form 0/0. As usual, it means that we have to consider the limit $\omega_{\text{sim}} \rightarrow \omega_{\text{max}}$. Expanding in Eq. (C.4) $|a_\ell^{(\text{PEC})}(\omega)|^2$ about the point $\omega_{\text{sim}} = \omega_{\text{max}}$ in powers of $\delta\omega = \omega_{\text{sim}} - \omega_{\text{max}}$ we readily obtain that

$$\lim_{\omega_{\text{sim}} \rightarrow \omega_{\text{max}}} \gamma = -\frac{\omega_{\text{max}}}{\sqrt{2}} \left\{ -1 + \sqrt{\frac{4}{\alpha^2 \omega_{\text{max}}^2} + 1} \right\}^{1/2}, \quad (\text{C.5})$$

where

$$\alpha^2 \equiv -\frac{1}{2|a_\ell^{(\text{PEC})}|_{\text{max}}^2} \left(\frac{\partial^2 |a_\ell^{(\text{PEC})}|_{\text{max}}^2}{\partial \omega^2} \right)_{\omega_{\text{max}}} > 0.$$

Appendix D: Overall dynamic

The comparison of the overall dynamic of the scattering obtained by the numerics [1] with that described by the models is presented in Figs. D.6 and D.7.

-
- [1] M. I. Tribelsky and A. E. Miroshnichenko, “Dynamics of destructive fano resonances,” *Phys. Rev. A*, vol. 100, p. 053824, Nov 2019.
- [2] W. H. Louisell, *Coupled mode and parametric electronics*. Wiley, 1960.

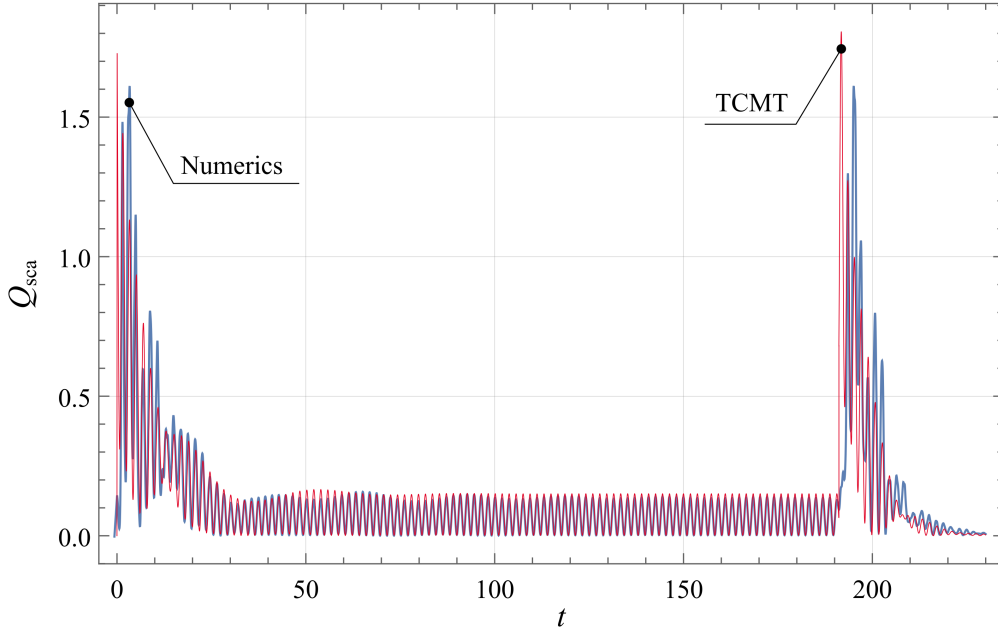


FIG. D.6. $Q_{\text{sca}}(t)$ obtained by the direct numeric integration of the complete set of Maxwell’s equations [1] and that described by the TCMT-model; $t = 0$ corresponds to the moment, when the scattered radiation for the first time is detected by the measuring monitors. The moment $t = \tau$ is clearly seen by the abrupt change of the dynamic from almost sinusoidal to essentially non-sinusoidal. Note the overshoot of the first oscillation behind both edges of the incident pulse (i.e., behind the points $t = 0$ and $t = \tau$) for the model relative to that for the numerics, explained by the instantaneous excitation of the background partition for the TCMT-model, see the discussion after Eq. (7) in the main text.

- [3] V. A. Mandelshtam and H. S. Taylor, “Harmonic inversion of time signals and its applications,” *The Journal of Chemical Physics*, vol. 107, no. 17, pp. 6756–6769, 1997.
- [4] P. Barone, E. Massaro, and A. Polichetti, “The segmented prony method for the analysis of non-stationary time series,” *Astronomy and Astrophysics*, vol. 209, pp. 435–444, 1989.
- [5] A. Roessling and J. Ringwood, “Finite order approximations to radiation forces for wave energy applications,” *Renewable energies offshore*, vol. 359, 2015.
- [6] C. F. Bohren and D. R. Huffman, *Absorption and Scattering of Light by Small Particles*. WILEY-VCH Verlag, 1998.

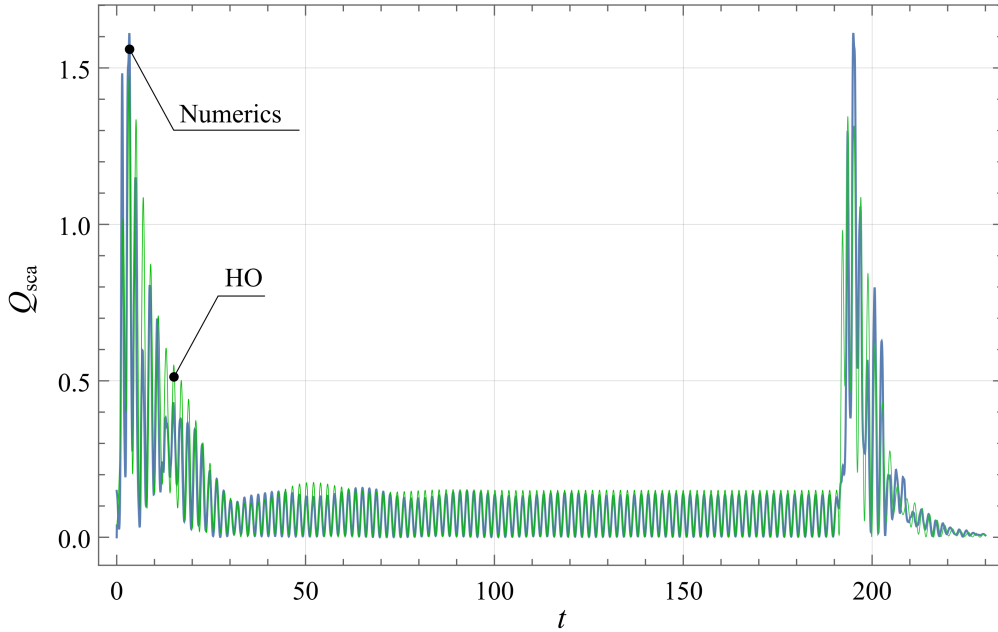


FIG. D.7. The same as that in Fig. D.6 for the HO-model. The overshoot does not occur.

- [7] A. E. Miroshnichenko, A. B. Evlyukhin, Y. F. Yu, R. M. Bakker, A. Chipouline, A. I. Kuznetsov, B. Luk'yanchuk, B. N. Chichkov, and Y. S. Kivshar, “Nonradiating anapole modes in dielectric nanoparticles,” *Nature Communications*, vol. 6, no. 1, p. 8069, 2015.
- [8] M. I. Tribelsky and A. E. Miroshnichenko, “Giant in-particle field concentration and fano resonances at light scattering by high-refractive-index particles,” *Physical Review A*, vol. 93, no. 5, p. 053837, 2016.
- [9] S. E. Svyakhovskiy, V. V. Ternovski, and M. I. Tribelsky, “Anapole: Its birth, life, and death,” *Optics express*, vol. 27, no. 17, pp. 23894–23904, 2019.
- [10] M. I. Tribelsky and A. E. Miroshnichenko, “Dynamics of destructive fano resonances,” *Physical Review A*, vol. 100, no. 5, p. 053824, 2019.
- [11] M. I. Tribelsky and A. E. Miroshnichenko, “Giant in-particle field concentration and fano resonances at light scattering by high-refractive-index particles,” *Physical Review A*, vol. 93, p. 053837, may 2016.
- [12] U. Fano, “On the absorption spectrum of noble gases at the arc spectrum limit,” *Nuovo Cimento*, vol. 12, pp. 154–161, 1935. <http://arXiv.org/abs/cond-mat/0502210v1>.

- [13] U. Fano, “Effects of configuration interaction on intensities and phase shifts,” *Phys. Rev.*, vol. 124, pp. 1866–1878, 1961.
- [14] A. E. Miroshnichenko, S. Flach, and Y. S. Kivshar, “Fano resonances in nanoscale structures,” *Reviews of Modern Physics*, vol. 82, no. 3, pp. 2257–2298, 2010.
- [15] Z. Ruan and S. Fan, “Temporal Coupled-Mode Theory for Fano Resonance in Light Scattering by a Single,” *The Journal of Physical Chemistry C*, vol. 114, no. 16, pp. 7324–7329, 2010.
- [16] L. Landau and E. Lifshitz, *Mechanics: Volume 1 (Course of Theoretical Physics Series)*, §23. Oxford Pergamon Press, Oxford, 2000.
- [17] M. I. Tribelsky, J.-M. Geffrin, A. Litman, C. Eyraud, and F. Moreno, “Small dielectric spheres with high refractive index as new multifunctional elements for optical devices,” *Scientific Reports*, vol. 5, no. 1, p. 12288, 2015.
- [18] M. I. Tribelsky, J.-M. Geffrin, A. Litman, C. Eyraud, and F. Moreno, “Directional fano resonances in light scattering by a high refractive index dielectric sphere,” *Phys. Rev. B*, vol. 94, p. 121110, Sep 2016.
- [19] M. I. Tribelsky, “Phenomenological approach to light scattering by small particles and directional fano's resonances,” *EPL (Europhysics Letters)*, vol. 104, p. 34002, nov 2013.